Eur. Phys. J. A (2025) 61:281
https://doi.org/10.1140/epja/s10050-025-01744-w

THE EUROPEAN PHYSICAL JOURNAL A

Regular Article - Experimental Physics

High-precision Q-value measurement and evaluation of nuclear matrix elements for ^{122}Sn and ^{124}Sn neutrinoless double beta decays

Elina Kauppinen[1,a], Jouni Ruotsalainen[1,b], Vikas Kumar[1,2], Jouni Suhonen[1,3], Anu Kankainen[1], Tommi Eronen[1], Jenni Kotila[4], Maxime Mougeot[1]

[1] Accelerator Laboratory, Department of Physics, University of Jyväskylä, P.O. Box 35 (YFL), 40014 Jyvaskyla, Finland
[2] Department of Physics, Banaras Hindu University, Varanasi, Uttar Pradesh 221005, India
[3] International Centre for Advanced Training and Research in Physics, P.O. Box MG12, 077125 Bucharest-Măgurele, Romania
[4] Finnish Institute for Educational Research, University of Jyväskylä, P.O. Box 35, 40014 Jyvaskyla, Finland

Received: 21 July 2025 / Accepted: 6 November 2025
© The Author(s) 2025
Communicated by Klaus Blaum

Abstract We have determined the decay energy (Q value) of the double beta decay of ^{122}Sn with the JYFLTRAP double Penning trap mass spectrometer using the Phase-Imaging Ion Cyclotron Resonance technique. Our new Q value, 373.58(12) keV, agrees with the literature value but is 20 times more precise. We also measured the Q value for the double beta decay of ^{124}Sn with unprecedented precision, 2293.542(83) keV. The Q values of ^{122}Sn and ^{124}Sn were used to calculate precisely the phase-space factors for the neutrinoless double beta ($0\nu\beta\beta$) decay mode of these nuclei. With the phase-space factor and our computed nuclear matrix elements (NMEs) we predict the $0\nu\beta\beta$-decay half-life of ^{122}Sn based on the recently extracted upper limit of the effective neutrino mass by the KamLAND-Zen experiment. We used three nuclear-structure frameworks to compute the NMEs, namely the proton-neutron quasiparticle random-phase approximation (pnQRPA), the microscopic interacting boson model (IBM-2), and a hybrid model exploiting both the pnQRPA and the nuclear shell model (NSM). We find that including the short-range components enhances the total NME in the IBM-2 model, making it significantly larger than the NMEs calculated with the pnQRPA and hybrid models. Nevertheless, for all models, the obtained half-lives are very long for ^{122}Sn ($\approx 10^{27}$–10^{29} years), making the observation of $0\nu\beta\beta$ decay of ^{122}Sn experimentally challenging. On the other hand, the hybrid-model calculated value of the NME for ^{124}Sn goes, interestingly enough, toward those previously computed by the NSM and the *ab initio* model.

1 Introduction

Double beta decay ($\beta^-\beta^-$) is a rare weak-interaction process, where two neutrons in the nucleus transform simultaneously into two protons [1], bypassing the energy barrier preventing a single beta decay from happening. It is known that the process can proceed via two modes: neutrinoless ($0\nu\beta^-\beta^-$) and two-neutrino ($2\nu\beta^-\beta^-$) decays [1]. In the already experimentally observed $2\nu\beta^-\beta^-$ mode [2], two electrons and electron antineutrinos are released from the nucleus. In contrast, in the $0\nu\beta^-\beta^-$ mode, no antineutrinos are released, and this constitutes a violation of the conservation of lepton number in the Standard Model of electroweak interactions. In addition, in order for the $0\nu\beta\beta$ decay to be possible, the neutrino should be its own antiparticle (so-called Majorana neutrino) and should have a non-zero effective mass $m_{\beta\beta}$, being a linear combination of the neutrino-mass eigenstates [1,3–5]. Observing the decay mode would thus be an indication of physics beyond the Standard Model, and hence all 0ν decays have recently been a subject of great interest in both nuclear and particle physics [5].

As the expected half-life of the $0\nu\beta^-\beta^-$ decay is on the order of 10^{28} yr for the so-called inverted mass ordering, choosing the right nucleus for experiments aiming to observe the decay is paramount. One of the most important factors in selecting the nucleus is the energy released in the decay known as the Q value. As the observation of $0\nu\beta\beta$ decay

[a] e-mail: elina.k.kauppinen@jyu.fi (corresponding author)
[b] e-mail: jouni.k.a.ruotsalainen@jyu.fi (corresponding author)

Published online: 11 December 2025

is based on measuring the kinetic energy of the emitted two electrons, a large Q value allows separating the $0\nu\beta^-\beta^-$ signal from the background consisting of various radioactive decay chains and the tail of the continuous $2\nu\beta^-\beta^-$ spectrum. In the $0\nu\beta^-\beta^-$ decay, a peak at the decay endpoint energy (Q value) in the energy spectrum of the sum of the electron kinetic energies would be an indication of the decay, while $2\nu\beta^-\beta^-$ decay results in a continuous spectrum till the endpoint energy.

The Q value is also essential for the calculation of half-life estimates to explore the feasibility of the decay modes. The expected half-life of the decay is inversely proportional to the fifth power of the Q value, and therefore the Q value should preferably be large and known with a high precision. Current double-beta experiments have focused on studying $\beta^-\beta^-$ decaying nuclei, as their half-lives are expected to be shorter than for the other double-beta-decay types. Notable currently ongoing and future experiments include CANDLES [6] for ^{48}Ca, LEGEND [7] for ^{76}Ge, SuperNEMO [8] for ^{82}Se, CUPID [9], AMoRE-II [10] and CROSS [11] for ^{100}Mo, CUORE [12] for ^{130}Te, and KamLAND-Zen [13], nEXO [14], NEXT [15], PandaX [16] and LZ [17] for ^{136}Xe.

While many current double-beta decay experiments focus on a few isotopes with favorable decay properties, such as large Q values and high natural abundances, a systematic investigation of a broader set of candidate nuclei remains crucial. Precision measurements of Q values across different isotopes refine nuclear data and serve as essential benchmarks for the theoretical models used to interpret the resulting double-beta decay data. Even isotopes such as ^{122}Sn, which have relatively low Q values and are not considered ideal for direct $0\nu\beta^-\beta^-$ searches, can contribute significantly to the field by enabling the cross-validation of experimental techniques and theoretical frameworks. In particular, comparative measurements of ^{124}Sn and ^{122}Sn provide valuable consistency checks for the JYFLTRAP setup, enhancing confidence in the reliability of the results obtained.

We have utilized the measured Q values to calculate phase-space factors for the decays of ^{122,124}Sn and computed the $0\nu\beta^-\beta^-$ nuclear matrix elements (NMEs) for the decay of ^{122}Sn using the microscopic interacting boson model (IBM-2), the proton-neutron quasiparticle random-phase approximation (pnQRPA), and the nuclear shell model (NSM). Estimates for these NMEs were still missing while the $2\nu\beta^-\beta^-$ NMEs for the ^{122}Sn decay were already computed using the pnQRPA model by Pirinen et al. [18] and Deppisch et al. [19]. With the new NMEs, we have also computed half-life estimates for the $0\nu\beta^-\beta^-$ decay of ^{122}Sn. The IBM-2 and NSM feature a small single-particle model space, typically one major shell between two neutron and proton magic numbers. This prevents both models to go beyond closure approximation in the double-beta-decay calculations, in particular in the present case. In this model space, the NSM can include, in principle, all the achievable many-nucleon configurations, whereas IBM-2 can only access configurations built using seniority 0 and 2 nucleon pairs. This makes the NSM more accurate for low-energy nuclear excitations. Contrary to those two models, pnQRPA features a large single-particle model space but a limited many-nucleon configuration space, like IBM-2. The notable advantage of pnQRPA is that it can be used for beyond-the-closure double-beta-decay calculations, in particular for the NMEs of the $0\nu\beta\beta$ decay.

Furthermore, this study introduces a novel new model, the hybrid model, used for both the ^{122}Sn and ^{124}Sn $0\nu\beta\beta$ decays. The hybrid model combines the strengths of the pnQRPA and NSM, and it is applied for the first time to $0\nu\beta\beta$ decay in this work. This new approach combines the ability of the NSM to produce reliable details of nuclear structure at relatively low excitation energies, below some few MeV. This strength of the NSM can be combined with the strong features of the pnQRPA being able to go to high excitation energies, even beyond the giant-resonance regions of nuclear excitations, the giant Gamow-Teller resonance being one example [20]. Hence, the hybrid model provides a complementary perspective to existing methods and helps explore the robustness of NME predictions across different modeling strategies, in particular if the model would be extended in the future to treatment of the most popular nuclei used in $0\nu\beta\beta$ experiments. At the same time, by extending the scope of experimental and theoretical studies to less commonly investigated isotopes such as ^{122}Sn, we promote a more comprehensive understanding of double-beta-decay systematics and support the development of future experimental programmes with broader isotope coverage.

For determining the Q value of radioactive decays, Penning-trap mass spectrometry has become the state-of-the-art method (see e.g. [21,22]). It has been used to measure, e.g., the $Q_{\beta^-\beta^-}$ of ^{98}Mo [23] and ^{96}Zr [24] and double electron-capture Q value for ^{190}Pt [25]. In this work, we applied the Phase-Imaging Ion Cyclotron Resonance (PI-ICR) method [26,27] at the JYFLTRAP double Penning trap setup [28] at the Ion Guide Isotope Separator On-Line (IGISOL) facility [29] to determine the Q value of ^{122}Sn $\beta^-\beta^-$ decay. The already well-known $Q_{\beta^-\beta^-}$ value of ^{124}Sn was also measured.

Since the NMEs for the ^{124}Sn have already been extensively studied, we are only performing the novel hybrid model calculations concerning that isotope. For reference, the $2\nu\beta^-\beta^-$ NMEs of ^{124}Sn have been addressed in [18,30] using the pnQRPA, in [31] using the NSM, and in [32,33] using the IBM-2 for both the ground-state and excited-state decays. For the ground-state transition the $0\nu\beta^-\beta^-$ NMEs for ^{124}Sn have been addressed using the NSM in [31,34] the pnQRPA in [30,35–38], the IBM-2 model in [32,33,39–41], an energy density functional in [42] and the beyond-mean-

field covariant density functional theory in [43]. Transition to the first excited 0^+ state has been treated using the NSM in [31], the pnQRPA in [30,37,44,45] and the IBM-2 in [32,33].

2 Experimental methods

We measured the $Q_{\beta^-\beta^-}$ values of ^{122}Sn and ^{124}Sn with the JYFLTRAP double Penning trap [28,46,47] at the IGISOL facility [29] in the Accelerator Laboratory of the University of Jyväskylä. The Q values were obtained by measuring the cyclotron frequency ratios of the singly-charged parent and daughter ions, ^{122}Sn-^{122}Te and ^{124}Sn-^{124}Te, respectively. The tin and tellurium ions were produced in two different electric discharge sources. The tellurium ions were produced in a source located inside the IGISOL target chamber, while the tin ions were created in the separate offline ion source station [48]. Ions from both sources were accelerated to 30 keV. An electrostatic bender was used to select ions from one source at a time while blocking the ions from the other source. The isotopes of interest were mass-separated using a dipole magnet with a mass resolving power $M/\Delta M \approx 500$ and sent to the radiofrequency quadrupole (RFQ) cooler-buncher [49,50]. In the cooler-buncher, the continuous ion beam was stopped and confined in the helium-filled volume, which allowed the ions to thermalize. After cooling, the captured ions were released as temporally narrow bunches, which could be efficiently injected into the JYFLTRAP double Penning trap.

The JYFLTRAP double Penning trap system consists of two Penning traps inside a 7 T superconducting solenoid [28]. First, the ion bunch from the cooler-buncher was captured in the helium-filled purification trap. There, the mass-selective buffer gas cooling [51] was performed to remove possible contaminant ions and prepare the ions-of-interest for transfer to the second trap, known as the measurement trap. The Phase-Imaging Ion Cyclotron Resonance (PI-ICR) method [26,46,47] was employed in the measurement trap to determine the free-space cyclotron frequency

$$\nu_c = \frac{1}{2\pi}\frac{q}{m}B, \tag{1}$$

where q and m are the charge and mass of the ion in the magnetic field strength B.

The Q value of the double-beta decay is obtained from the cyclotron frequency ratio between the singly-charged double-beta decaying parent (p) and its daughter (d) ions, $r = \nu_{c,d}/\nu_{c,p}$, as

$$\begin{aligned} Q_{\beta^-\beta^-} &= (m_p - m_d)c^2 \\ &= (m_d - m_e)(r-1)c^2 + (r\cdot B_d - B_p), \end{aligned} \tag{2}$$

where m_p and m_d are the atomic masses of the parent and the daughter isotopes, m_e is the electron mass, and B_d and B_p are the binding energies of the outermost electron in the daughter and the parent atoms. Since the term $r \cdot B_d - B_p$ is small ($\sim$2 eV [52]) compared to the experimental uncertainty, it has been neglected in the analysis.

In the PI-ICR technique, the cyclotron frequency is obtained as the sum of the magnetron (ν_-) and reduced cyclotron (ν_+) frequencies, $\nu_c = \nu_- + \nu_+$. These radial frequencies are obtained by measuring the phases of the two motions after a certain phase accumulation time t_{acc}. The measurements are performed by projecting the ions onto a position-sensitive microchannel plate detector, which leads to a so-called phase spot for each of the motions, see e.g. Ref. [47] for details. With the difference in the angles of the measured magnetron (α_-) and cyclotron (α_+) spots relative to the center, we obtain the cyclotron frequency of the ion species as

$$\nu_c = \frac{(\alpha_+ - \alpha_-) + 2\pi n_c}{2\pi t_{acc}}, \tag{3}$$

where n_c is the number of turns the ions would perform during the accumulation time t_{acc} at the frequency ν_c. Figure 1 shows an example of the measured magnetron (α_-) and cyclotron (α_+) spots for $^{122}Sn^+$.

To determine the $Q_{\beta^-\beta^-}$ value of ^{122}Sn, altogether 56 frequency ratios were measured against the $^{122}Te^+$ daughter ions over 14 h. A weighted average $\bar{r}$, with the larger of the internal and external error [53] as the uncertainty, was taken as the final frequency ratio. An accumulation time of 1135 ms was used in the measurements, with the exact time set to be an integer multiple of the period of ν_c. This minimizes the difference in the magnetron and reduced cyclotron spot angles, reducing the systematic shift of the ratio caused by differences in ion trajectories. To minimize the effect of the magnetic field fluctuation, measured to be $\delta B/(B\delta t) = 2.01 \times 10^{-12}$ min^{-1} [47], measurements of the parent and the daughter cyclotron frequencies were done in alternating order, switching between the species every 8 min. The magnetic field strength at the middle of the frequency measurement of the daughter was then linearly interpolated from the measurement of the parent's cyclotron frequency. Before applying the excitations in the PI-ICR measurement cycle, the ions are centered in the precision trap by driving the magnetron motion to zero. To average over any magnetron motion left over from the centering, the start of the excitation pulse at ν_+ was scanned over one magnetron period ($\sim$600 µs) and similarly, any residual cyclotron motion of the extracted ions was averaged by scanning the extraction delay from the trap over one cyclotron period ($\sim$1 µs). A similar treatment was done to measure the already well-known $Q_{\beta^-\beta^-}$ value of ^{124}Sn to cross-check the performance of the

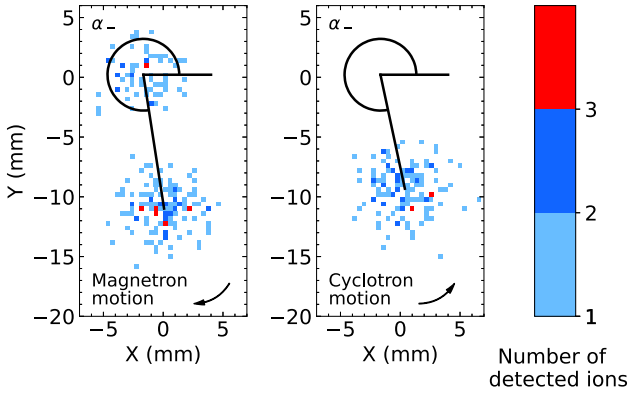

Fig. 1 The final phases of the magnetron and cyclotron motions and their measured angles α_- and α_+ with respect to the trap centre on the microchannel plate detector for $^{122}Sn^+$ ions after an accumulation time of 1135 ms. The data are from a ≈ 8-min measurement

JYFLTRAP mass spectrometer. For this case, 103 ratios over 24 h were measured using an accumulation time of 1015 ms.

3 Experimental results

The measured frequency ratios and the resulting Q values are presented in Table 1 and Fig. 2 We provide the first direct measurement of the $Q_{\beta^-\beta^-}$ value for ^{122}Sn. The determined $Q_{\beta^-\beta^-}$ is 373.58(12) keV, which is in line with the value given in the Atomic Mass Evaluation 2020 (AME20) [54], 373.3(24) keV, but 20 times more precise. We also improve the precision for the mass-excess (ME) value of ^{122}Sn, yielding $ME = -89939.7(14)$ keV. In the AME20, the ME value of ^{122}Sn is based on the $^{122}\mathrm{Sn}(d,t)^{121}\mathrm{Sn}$ [55] and $^{122}\mathrm{Sn}(n,\gamma)^{123}\mathrm{Sn}$ [56,57] reactions, while ^{122}Te is linked via (n,γ) measurements [58–61] to the mass of ^{124}Te determined with SHIPTRAP Penning trap in [62], see Ref. [63] for details.

For ^{124}Sn, we obtained a frequency ratio $\bar{r} = 1.00001987\,227(72)$ and $Q_{\beta^-\beta^-} = 2293.542(83)$ keV, which is 0.84(41) keV larger but within two standard deviations (2σ) from the AME20 value [54]. The AME20 value is based mainly on a measurement performed with the SHIPTRAP Penning trap [62], as the SHIPTRAP value, $Q_{\beta^-\beta^-} = 2292.64(39)$ keV [62], is much more precise and deviates from the earlier measurement done using the Manitoba II mass spectrometer by 2.6(1.0) keV. With the PI-ICR method and measured 103 frequency ratios, our precision is nearly 5 times better than obtained at SHIPTRAP with their 36 frequency ratios measured using the time-of-flight ion cyclotron resonance (ToF-ICR) technique [64,65] applying a Ramsey excitation pattern [66,67] of 25–950–25 ms. The agreement within 2σ is reasonable. It is worthwhile to note that on one hand, also for the $Q_{\beta^-\beta^-}$ of ^{130}Te reported in Ref. [62], around 0.6(3) keV deviation was found to the earlier JYFLTRAP [68] and Canadian Penning Trap measurements [69], which agreed very well with each other. On the other hand, there are several cases where the SHIPTRAP and JYFLTRAP results agree with each other, such as the double electron-capture Q value for ^{102}Pd [70–72].

4 Theoretical methods and results

The half-life for the neutrinoless double beta decay can be written as

$$T^{0\nu}_{1/2} = \left(g_{\mathrm{A}}^4 G_{0\nu} |M^{(0\nu)}|^2 \frac{m^2_{\beta\beta}}{m^2_e} \right)^{-1}, \tag{4}$$

where g_{A} is the (effective) axial vector coupling, $G_{0\nu}$ and $M_{0\nu}$ are the phase space factor and nuclear matrix element (NME), respectively, for $0\nu\beta\beta$ decay, $m_{\beta\beta}$ is the effective mass of the neutrino and m_e is the electron rest mass.

The phase-space factor for the $0\nu\beta^-\beta^-$ decay is calculated using the newly measured, very precise Q value of the decay as explained in detail in Ref. [73]. For the calculation of the phase-space factors, the wave functions of the two electrons emitted in the double beta decay are needed. The wave functions are derived from exact Dirac solutions, taking into account finite nuclear size and electron screening. The value for the $0\nu\beta^-\beta^-$ phase-space factor for ^{122}Sn was calculated to be $G_{0\nu} = 7.76 \times 10^{-17}$ yr^{-1}. Since there is only a minor difference between the new and old Q values, the phase-space factor is not greatly affected by the new Q value. However, as the new Q value is much more precise, the margin of error when calculating the phase-space factor has been significantly reduced. The error of the Q value is directly related to phase-space factor uncertainty in neutrinoless double beta decay, as $3 \times \delta Q/Q$ as stated in Ref. [73]. With the older Q value of 373.3(24) keV, the uncertainty in the phase-space factor cumulates to 1.9%. With the new, more precise value of 373.58(12) keV, the uncertainty in the phase-space factor due to the Q value is now reduced to 0.096%.

Also, the phase-space factor for the $0\nu\beta^-\beta^-$ decay of ^{124}Sn was calculated with the new Q value. The new phase-space factor was calculated to be 9.13×10^{-15} yr^{-1}. This phase-space factor was studied earlier in [73], and it was calculated to be 9.04×10^{-15} yr^{-1}. The slight difference in the phase-space factors is due to a small increase in the measured Q value. As in the case of ^{122}Sn, the uncertainty of the phase-space factor cumulating from the measured Q value can be estimated. For ^{124}Sn phase-space factor, the uncertainty from the Q value is 0.011%, making it negligible compared to other sources of uncertainty; the estimated radius R (7%) and used electron screening model (0.10%)[73].

Table 1 The mean frequency ratios $\bar{r}$ between the daughter and the parent ions, and the corresponding Q values, $Q_{\beta^-\beta^-}(^{122}\mathrm{Sn})$ and $Q_{\beta^-\beta^-}(^{124}\mathrm{Sn})$, determined in this work. The literature values from Ref. [54] and the differences between the measured and the literature values are also shown

Parent	Daughter	$\bar{r}$	Q (keV)	$Q_{lit.}$ (keV)	ΔQ (keV)
^{122}Sn	^{122}Te	1.0000032899(10)	373.58(12)	373.3(24)	0.28(240)
^{124}Sn	^{124}Te	1.00001987227(72)	2293.542(83)	2292.7(4)	0.842(409)

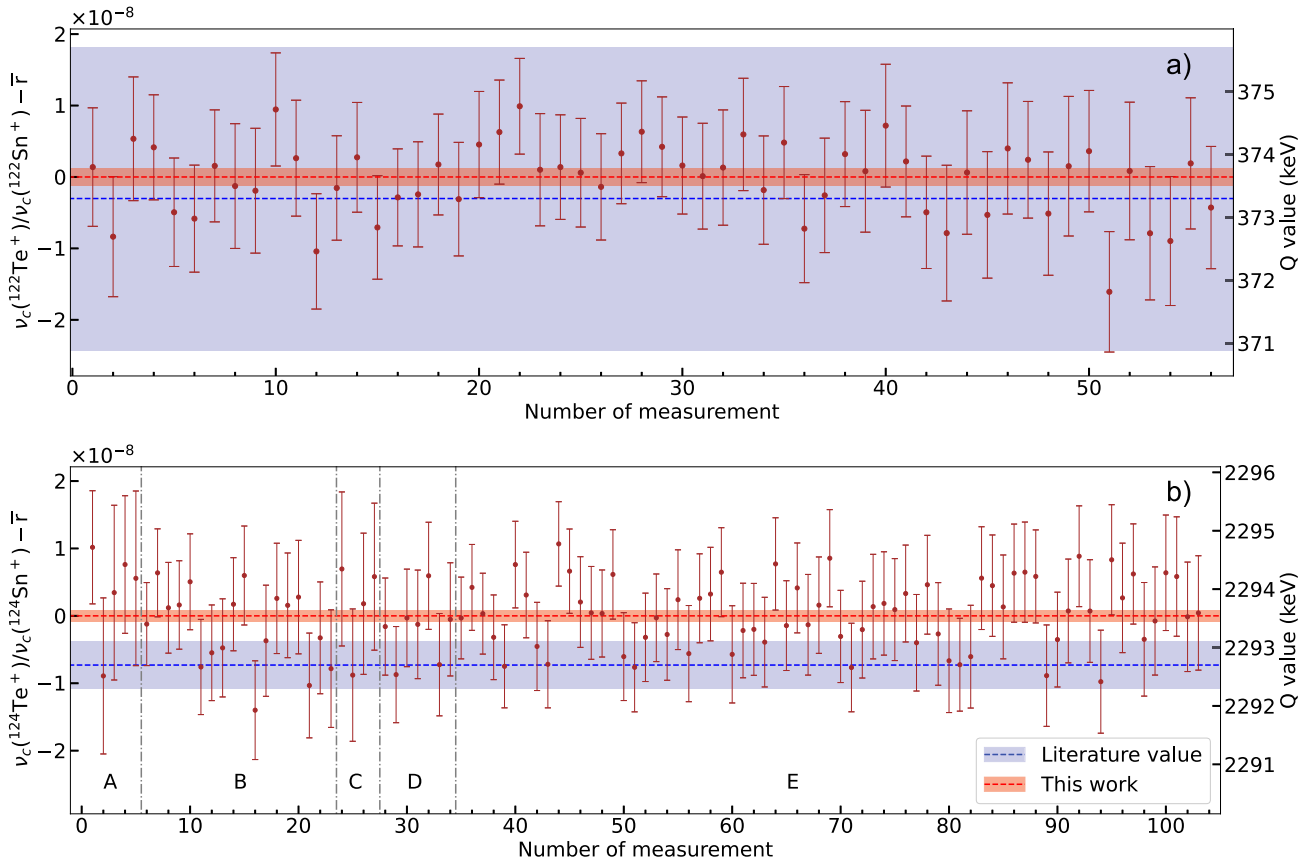

Fig. 2 The individual measured frequency ratios from which the weighted average $\bar{r}$ has been subtracted, and the corresponding $Q_{\beta^-\beta^-}$ values. The red band indicates the uncertainty of the measured ratio, taken to be the larger of the internal and external errors, while the blue band indicates the Q value given in [54]. In (**a**), an accumulation time of 1135 ms was used, while in (**b**), an accumulation time of 1015 ms was used. The vertical dashed lines in (**b**) indicate breaks in the measurement and adjustment of the excitation frequencies

Another key factor in studying $0\nu\beta^-\beta^-$ decay is the NME. We have calculated the NME of the $0\nu\beta^-\beta^-$ decay of ^{122}Sn using the microscopic interacting boson model (IBM-2), the proton-neutron quasiparticle random-phase approximation (pnQRPA), and the so-called hybrid model, which combines the nuclear shell model (NSM) and pnQRPA.

For the $0\nu\beta^-\beta^-$ decay NME, the Gamow–Teller (GT), Fermi (F), and tensor (T) matrix elements are needed. The NME can then be constructed as

$$M^{(0\nu)} = \pm\left(\frac{g_V}{g_A}\right)^2 M_F \mp M_{GT} + M_T, \tag{5}$$

where the upper signs are used for the IBM-2 [40] and lower signs for pnQRPA and the hybrid model [36]. It should be noted that the relative sign of the tensor term differs depending on whether the calculation is performed in momentum or coordinate space, as discussed in Ref. [74]. Here $g_V = 1.0$ is the vector coupling. The bare value of the axial-vector coupling $g_A = 1.27$ was chosen in our analyses. Also, the Jastrow-type short-range correlation (SRC) was used with the CD-Bonn parametrization. The SRC can be applied to wave functions to take into account the nuclear repulsive force at short distances, thus making the NME calculation

more realistic. The used SRC is of the form

$$f(r) = 1 - ce^{-ar^2}(1 - br^2), \tag{6}$$

where r represents the relative distance between the two nucleons and the used parameter values are $a = 1.52$ fm^{-2}, $b = 1.88$ fm^{-2}, and $c = 0.46$ [75].

Our shell-model calculations were conducted with the sn100pn interaction [76,77] in the $50 - 82$ valence major shell, which includes the orbits $0g_{7/2}$, $1d_{5/2}$, $0h_{11/2}$, $2s_{1/2}$, and $1d_{3/2}$. The sn100pn interaction has four parts; neutron-neutron, neutron–proton, proton–proton and Coulomb repulsion between the protons. For neutrons, the single-particle energies (SPEs) are -10.608, -10.289, -8.717, -8.694, and -8.816 MeV for $0g_{7/2}$, $1d_{5/2}$, $1d_{3/2}$, $2s_{1/2}$ and $0h_{11/2}$ orbitals, respectively. For protons, the SPEs are 0.807, 1.562, 3.316, 3.224, and 3.605 MeV for $0g_{7/2}$, $1d_{5/2}$, $1d_{3/2}$, $2s_{1/2}$, and $0h_{11/2}$ orbitals, respectively. The NuShellX@MSU [78] code has been used to diagonalize the energy matrices of the NSM. To reduce the computational burden, we have employed truncations for the neutron orbitals. The orbital $\nu\, 0g_{7/2}$ was left completely filled, and we forced a minimum of four particles in the $\nu 1d_{5/2}$ orbital. No truncations were applied for the proton occupancies.

The pnQRPA calculations were performed in the way described in the $0\nu\beta^-\beta^-$-decay calculations of Jokiniemi et al. [79] (see a general account on the use of pnQRPA-type theories in this context in [1, p. 31]). The single-particle valence space consisted of three major shells, $1p0f - 2s1d0g - 2p1f0h$, including 15 single-particle orbitals for both protons and neutrons. All spin-orbit partners were included in the single-particle model space. The single-particle energies were obtained from the Woods–Saxon mean-field potential [80], and the Hamiltonian was based on the Bonn one-boson-exchange G-matrix [81], fine-tuned in its isoscalar part by the particle-particle interaction parameter $g_{\rm pp}(T = 0) = 0.91$ and in its isovector part by $g_{\rm pp}(T = 1) = 0.94$. The particle-hole parameter was set to the bare G-matrix value $g_{\rm ph} = 1.0$. The pairing part was adjusted separately in the even-even reference nuclei ^{122}Sn and ^{122}Te to yield the proton (neutron) pairing strength $g_{\rm pair} = 1.07$ ($g_{\rm pair} = 1.06$) in ^{122}Sn and $g_{\rm pair} = 1.03$ ($g_{\rm pair} = 1.01$) in ^{122}Te. Since the intermediate J^π states were calculated using both the initial and final $0\nu\beta^-\beta^-$-decay nuclei as reference nuclei, the expression for the $0\nu\beta^-\beta^-$-decay amplitude has to contain an overlap factor in order to achieve a state-by-state matching, see, e.g., the review [3].

The cumulative NME of ^{122}Sn $0\,\nu\,\beta^-\,\beta^-$ decay is shown in Fig. 3, obtained utilizing a hybrid technique (NSM + pnQRPA) and the extreme values of the low-energy constants (LEC) of the included meson-exchange two-body currents (2BC) (hatched region). These 2BC are the same as utilized in the ordinary muon capture (OMC) in the work of Gimeno et al. [82], exploiting the reduction of the 2BC to an effective one-body current in the Fermi-sea approximation [83]. Since the NSM is more accurate for low excitation energies than the pnQRPA, we have treated the excited states in the intermediate nucleus ^{122}Sb up to some 1.5 MeV of excitation by the NSM. Upward from this cut-off, marking the saturation of the NSM cumulative strength, we continued with the pnQRPA-computed nuclear wave functions. By means of this procedure, we are able to combine the precision of the low-energy description of the NSM with the capability of the pnQRPA in describing high-energy excitations up to and beyond the giant-resonance regions. For a pure pnQRPA calculation, Fig. 4 shows the cumulative NME of ^{122}Sn $0\,\nu\,\beta\,\beta$ decay without the 2BC, but with the positive- and negative-parity components separated. This is to demonstrate that the 1^+ Gamow-Teller giant resonance is the source of the negative contribution around 13 MeV.

In the IBM-2 nuclear many-body framework, the nucleus is considered to consist of an inert core and valence nucleons. The core and valence nucleons are separated by the closest magic shell for both protons and neutrons. The valence nucleons above or holes below the magic shell are considered to pair up to create bosonic particles or holes with angular momentum and parity of 0^+ and 2^+, the so-called s- and d-bosons. The relevant equations and derivation for the IBM-2 can be found in Ref. [84]. In IBM-2 calculations, the isospin restoration formalism and closure approximation are used. In neutrinoless double beta decay, the closure approximation has only a minor effect on the final results since the closure energy is much smaller than the typical neutrino momentum [32]. Nevertheless, it greatly simplifies the computational process by eliminating the need to explicitly sum over intermediate nuclear states. The IBM-2 Hamiltonian parameters used in this work are shown in Table 2, and the single particle energies used in the mapping are taken from Ref. [85].

In addition to long-range NME calculations, we have proceeded with novel calculations for the short-range component of the NME of the $0\nu\beta^-\beta^-$ decay using the IBM-2 framework. This component was recently found to be of importance in Ref. [86] and was shown to be a crucial part of the total NME of neutrinoless double beta decay. In ab initio calculations [87], it was shown that the new short-range component enhances the total nuclear matrix element. Therefore, it can be taken into account as an additional contribution to the NME by summing the long-range and short-range components of the NME together as

$$M_{tot} = M_L + M_S, \tag{7}$$

where M_L is the long-range NME and M_S is the short-range NME. For the calculation of short-range NMEs, we adopted the same set of plausible parameters as those used in Ref. [38]. It should be noted that these parameters cannot currently

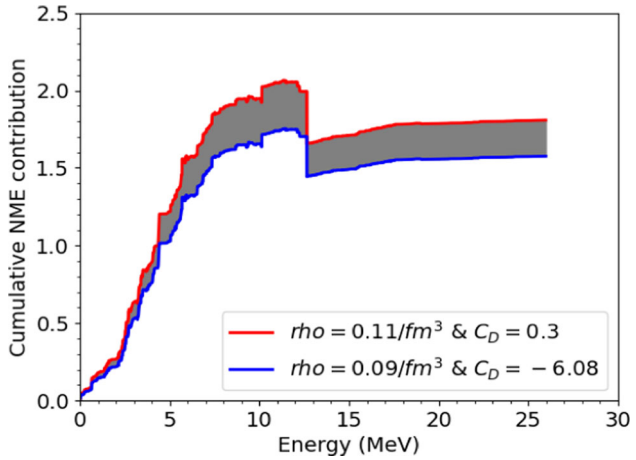

Fig. 3 Cumulative value of the $0\nu\beta^-\beta^-$ decay NME of ^{122}Sn in the hybrid model (NSM + pnQRPA) with 2BC included as a function of the excitation energy in the intermediate nucleus. The insert shows the extreme values of the LECs [82] adopted in the computations

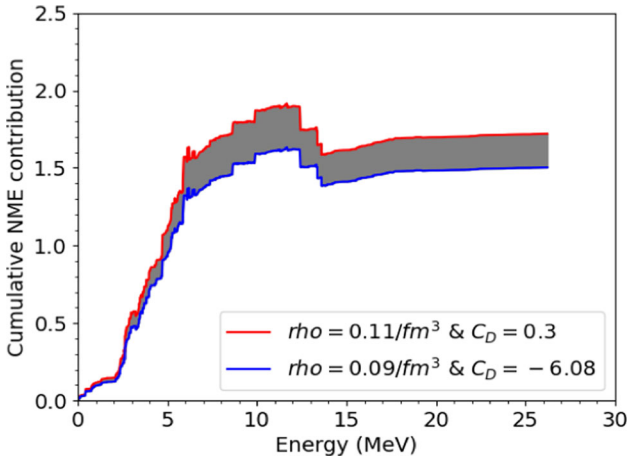

Fig. 5 Cumulative value of the $0\nu\beta^-\beta^-$ decay NME of ^{124}Sn in the hybrid model (NSM + pnQRPA) with 2BC included as a function of the excitation energy in the intermediate nucleus. The insert shows the extreme values of the LECs [82] adopted in the computations

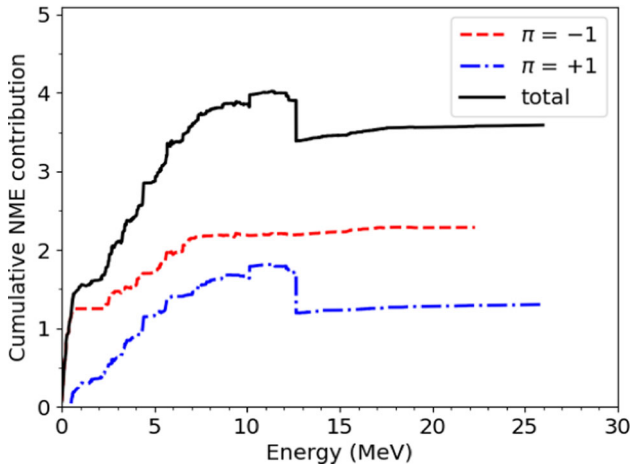

Fig. 4 Cumulative value of the pnQRPA-computed NME (without 2BC) of ^{122}Sn as a function of the excitation energy in the intermediate nucleus. For more information, the contributions of the negative-parity ($\pi = -1$) and positive-parity ($\pi = +1$) have been separated

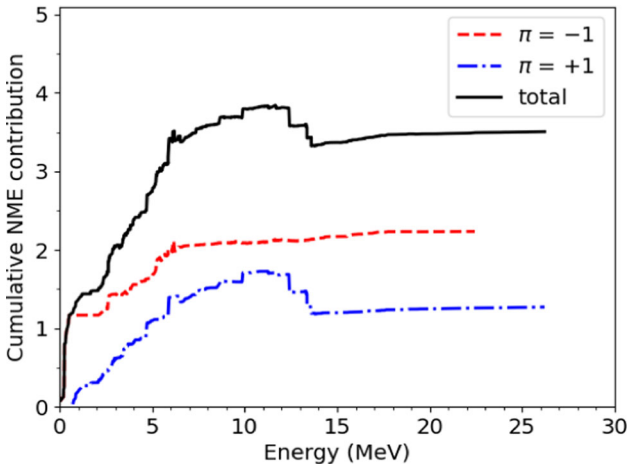

Fig. 6 Cumulative value of the pnQRPA-computed NME (without 2BC) for ^{124}Sn as a function of the excitation energy in the intermediate nucleus. For more information, the contributions of the negative-parity ($\pi = -1$) and positive-parity ($\pi = +1$) have been separated

be determined from experimental data, and therefore, the resulting short-range NME values should be interpreted as theoretical estimates. The calculated values for the individual NMEs and the total NME for ^{122}Sn are shown in Table 3.

As shown in Table 3, the calculated NMEs for the ^{122}Sn using different nuclear models differ quite a bit. The IBM-2 gives the highest values, the hybrid model the lowest, and pnQRPA lies in between those. Using 2BCs lowers the NME values in pnQRPA and hybrid model calculations by about 20–35 % depending on the used parameters. In IBM-2 calculations, adding the short-range component to the total NME enhances the NME by approximately 20–40 %, depending on the parameters.

The half-lives of the decay can be calculated using Eq. (4) and inserting the NMEs obtained with different nuclear models. In Fig. 7, minimum half-life estimates are presented. The mass range for the used effective neutrino mass $m_{\beta\beta}$ is 0.036–0.156 eV, which is obtained using the currently most stringent half-life limit from the KamLAND-Zen experiment [88]. The effective neutrino mass limits are extracted from the half-life limit by the use of Eq. (4), the phase-space factor for the decay, and the NMEs calculated with different nuclear models, as explained in [88], giving the upper limits for the effective neutrino mass. The half-life limit from the KamLAND-Zen experiment is also visible in Fig. 7. It includes half-lives obtained with the NMEs using pnQRPA and the hybrid model, with and without the 2BCs, and also the IBM-2 results, using only the usual long-range NME and the total NME where long- and short-range NMEs are summed together.

Table 2 Parameters used in the IBM-2 Hamiltonian for ^{122}Sn and ^{122}Te

Nucleus	ϵ_{d_ν}	ϵ_{d_π}	κ	χ_ν	χ_π	$c_\nu^{(0)}$	$c_\nu^{(2)}$	$c_\nu^{(4)}$	w_ν	y_ν
^{122}Sn	1.14					− 0.19	0.5	− 0.10	− 0.01	0.02
^{122}Te	0.8	0.8	− 0.12	− 0.25	− 1.20					

Table 3 Neutrinoless double beta decay NMEs for ^{122}Sn calculated with pnQRPA, IBM-2, and the hybrid model. In the pnQRPA and hybrid model calculations, the NMEs are obtained with and without 2BCs. In the IBM-2 model, the short-range component of the NME is also calculated

	pnQRPA		IBM-2	Hybrid	
	wo2BC	2BC		wo2BC	2BC
$M_F^{(0\nu)}$	1.394	1.394 to 1.394	0.704	1.081	1.081 to 1.081
$M_{GT}^{(0\nu)}$	− 2.965	− 1.504 to − 1.909	− 3.606	− 1.614	− 0.817 to − 1.028
$M_T^{(0\nu)}$	0.239	0.099 to 0.122	0.153	0.308	0.129 to 0.158
$\lvert M^{(0\nu)}\rvert$	3.589	2.268 to 2.651	4.196	1.976	1.574 to 1.808
$\lvert M_S^{(0\nu)}\rvert$	–	–	0.811 to 1.743	–	–

Table 4 Neutrinoless double beta decay NMEs for ^{124}Sn calculated with pnQRPA and the hybrid model. In the pnQRPA and hybrid model calculations, the NMEs are obtained with and without 2BCs

	pnQRPA		Hybrid	
	wo2BC	2BC	wo2BC	2BC
$M_F^{(0\nu)}$	1.368	1.368 to 1.368	1.058	1.058 to 1.058
$M_{GT}^{(0\nu)}$	− 2.899	− 1.468 to − 1.865	− 1.692	− 0.853 to − 1.083
$M_T^{(0\nu)}$	0.242	0.101 to 0.124	0.295	0.123 to 0.152
$\lvert M^{(0\nu)}\rvert$	3.506	2.216 to 2.590	2.053	1.502 to 1.721

Although the achievable sensitivity of an experiment observing the $0\nu\beta^-\beta^-$ decay depends on the experimental setup and the properties of the nucleus, in particular the decay Q value, the estimated half-lives of ^{122}Sn significantly exceed the current experimental sensitivity, as shown in Fig. 7. This is primarily due to the very low Q value of the decay, which substantially suppresses the phase-space factor.

The hybrid model calculations are also performed for the decay of ^{124}Sn and the cumulative values for the NMEs are represented in Figs. 5 and 6. The values for the NMEs are also shown in Table 4. Since the $0\nu\beta\beta$ decay in ^{124}Sn has been extensively studied, many references to NME values are already available. The NMEs obtained by using the hybrid model are plotted among other nuclear model calculations in Fig. 8. As already observed for the ^{122}Sn decay, the NMEs calculated with the hybrid model have lower values compared to the pnQRPA results. Incorporating the 2BCs further lowers the NME value as for ^{122}Sn. When compared to other models in Fig. 8, the hybrid-model NME, without the 2BCs, is close to the NSM-computed one of Menendez et al. [34]. Adding the 2BCs to the hybrid NME brings the hybrid NME the lowest of all the other NMEs. Interestingly, this goes toward the effect of the ab initio calculations on the values of $0\nu\beta\beta$ NMEs for masses below $A = 82$ obtained in Belley et al. [89]: the ab initio and hybrid-model NMEs seem to be the smallest of all for the $0\nu\beta\beta$-decaying nuclei. Hence, the hybrid model gives a highly complementary view on the palette of the available NMEs, leaning toward the NME estimates of the NSM and ab initio theory.

5 Conclusions

In this work, the $Q_{\beta^-\beta^-}$ value of ^{122}Sn was measured to be 373.58(12) keV, agreeing with the AME20 value while being 20 times more precise. The $Q_{\beta^-\beta^-}$ of ^{124}Sn was also measured, resulting in an agreement at the 2σ level with AME20, while being nearly 5 times more precise. These highly precise $Q_{\beta^-\beta^-}$ values for ^{122}Sn and ^{124}Sn were used to calculate the phase-space factors for the $0\nu\beta\beta$ decay mode, leading to significantly improved PSF accuracy. The involved NMEs were also computed using three different nuclear models: The pnQRPA, the hybrid model, which mixes the NSM and pnQRPA, and, finally, IBM-2.

The calculation of NMEs using pnQRPA and the hybrid model was done with and without 2BCs. The effect of 2BC

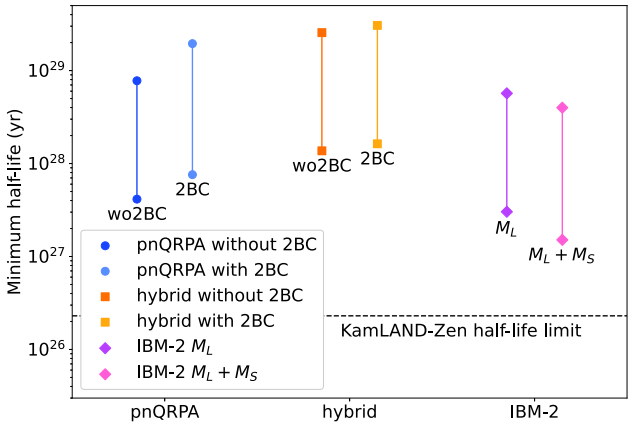

Fig. 7 Minimum values for the ^{122}Sn $0\nu\beta^-\beta^-$-decay half-lives using the pnQRPA, hybrid model, and IBM-2. For the pnQRPA and hybrid model, the NMEs with and without the 2BCs are used, and for IBM-2, both long-range and the sum of the long- and short-range NMEs are used to calculate the half-lives. The effective neutrino mass range was set to be 0.036–0.156 eV, which is obtained from the KamLAND-Zen half-life limit [88], which is also presented in the figure

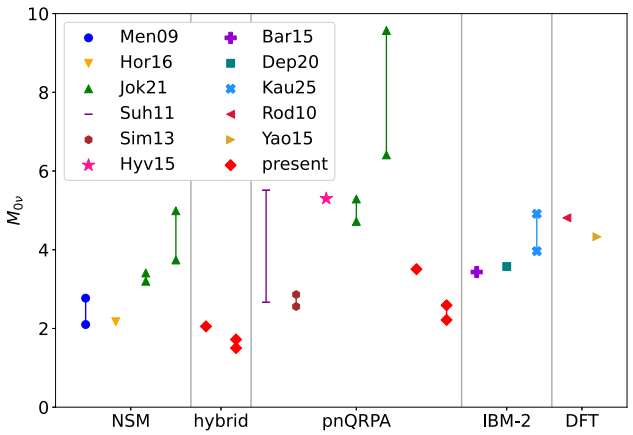

Fig. 8 Neutrinoless double beta decay NMEs for ^{124}Sn. Calculations done by the hybrid model and pnQRPA are labeled as present in the figure, and they contain the results obtained both with (the vertical range) and without (the single mark) the 2BCs. The figure contains calculations done by using NSM in Men09 [34], Hor16 [31], and Jok21 [38], pnQRPA in Suh11 [30], Sim13 [35], and Hyv15 [36], IBM-2 in Bar15 [33] (with sign change in the tensor part as indicated in [40]), Dep20 [40], and Kau25 [41], and density functional theory (DFT) based models Rod [42] and Yao15 [43]. The NSM and pnQRPA results from Jok21 include the usual long-range NME and the sum of the short- and long-range NMEs. The IBM-2 result in Kau25 presents also the sum of long- and short-range NMEs

is very noticeable, and the NMEs with 2BC are smaller, as found in other studies as well [90]. The hybrid model, based on both the NSM and pnQRPA calculations, also gives a smaller total NME when compared to that of pure pnQRPA. This is because the NSM gives smaller contributions at low excitation energies of the intermediate nucleus of the $0\nu\beta^-\beta^-$ decay than the pnQRPA. Interestingly, the magnitudes of the hybrid-model NMEs converge toward those of the nuclear shell model and the ab initio model. When using the IBM-2 nuclear model, the short-range component of the NME was also calculated. Depending on the chosen parameters, this short-range contribution can amount to more than 40% of the long-range NME. Its inclusion significantly enhances the total $0\nu\beta^-\beta^-$ NME, resulting in values that are considerably larger than those obtained using the pnQRPA and hybrid models. The potential impact and enhancement due to the short-range component on the total $0\nu\beta^-\beta^-$ nuclear matrix element (NME) has been investigated in several previous studies [38,41,86,91], with recent results suggesting that it contributes significantly to the total NME.

With the use of the computed NMEs and the evaluated phase-space factor, half-life estimates of the $0\nu\beta^-\beta^-$ decay of ^{122}Sn could be made. Using the upper effective neutrino mass limit, 0.156 eV, obtained in [88], the lower estimates for the half-life range from 1.51×10^{27} to 1.63×10^{28} years, depending on the nuclear model used. Unfortunately, no experimental limits on the half-life are currently available. Since the estimated half-lives are very long, exceeding the highest experimental half-life limit, observing neutrinoless double-beta decay of ^{122}Sn is likely to be difficult. With the new precise Q value, ^{122}Sn can be used to test the theoretical and experimental frameworks used in double-beta decay studies.

Acknowledgements E.K. and J.R. acknowledge the support from the Vilho, Yrjö and Kalle Väisälä foundation. J.K. and J.S. acknowledge support from project PNRR-I8/C9-CF264, Contract No. 760100/23.5. 2023 of the Romanian Ministry of Research, Innovation and Digitization (the NEPTUN project). V.K. acknowledges financial support from 'GEFP' IoE BHU fellowship (R/Dev/D/IoE/2024-25/GEFP/76559), and SERB Project (File No. EEQ/2023/000157), Govt. of India. A.K. acknowledges support from the Research Council of Finland under the grant No. 354968.

Funding Open Access funding provided by University of Jyväskylä (JYU).

Data Availability Statement Data will be made available on reasonable request. [Authors' comment: The experimental data analysed in the current study will be made available from the institutional repository and is available from the corresponding author on reasonable request.]

Code Availability Statement Code/software cannot be made available for reasons disclosed in the code availability statement. [Authors' comment: The codes/software generated during the current study is not publicly available since they are not meant for public use, e.g., due to the lack of user-friendly documentation for the use of the several interconnected computer codes.]

Open Access This article is licensed under a Creative Commons Attribution 4.0 International License, which permits use, sharing, adaptation, distribution and reproduction in any medium or format, as long as you give appropriate credit to the original author(s) and the source, provide a link to the Creative Commons licence, and indicate if changes were made. The images or other third party material in this article are included in the article's Creative Commons licence, unless indi-

cated otherwise in a credit line to the material. If material is not included in the article's Creative Commons licence and your intended use is not permitted by statutory regulation or exceeds the permitted use, you will need to obtain permission directly from the copyright holder. To view a copy of this licence, visit http://creativecommons.org/licenses/by/4.0/.

References

1. H. Ejiri, J. Suhonen, K. Zuber, Neutrino–nuclear responses for astro-neutrinos, single beta decays and double beta decays. Phys. Rep. **797**, 1–102 (2019). https://doi.org/10.1016/j.physrep.2018.12.001
2. A.S. Barabash, Precise half-life values for two-neutrino double-β decay: 2020 review. Universe **6**(10), 159 (2020). https://doi.org/10.3390/universe6100159. arXiv:2009.14451 [nucl-ex]
3. J. Suhonen, O. Civitarese, Weak-interaction and nuclear-structure aspects of nuclear double beta decay. Phys. Rep. **300**(3–4), 123–214 (1998). https://doi.org/10.1016/s0370-1573(97)00087-2
4. J. Engel, J. Menéndez, Status and future of nuclear matrix elements for neutrinoless double-beta decay: a review. Rep. Prog. Phys. **80**(4), 046301 (2017). https://doi.org/10.1088/1361-6633/aa5bc5
5. M. Agostini, G. Benato, J.A. Detwiler, J. Menéndez, F. Vissani, Toward the discovery of matter creation with neutrinoless $\beta\beta$ decay. Reviews of Modern Physics **95**(2) (2023). https://doi.org/10.1103/revmodphys.95.025002
6. S. Ajimura et al. (CANDLES Collaboration), Low background measurement in CANDLES-III for studying the neutrino-less double beta decay of ^{48}Ca. Phys. Rev. D **103**, 092008 (2021)
7. N. Abgrall et al. (LEGEND Collaboration), The Large Enriched Germanium Experiment for Neutrinoless $\beta\beta$ Decay: LEGEND-1000 preconceptual design report. arXiv:2107.11462 [physics.ins-det]
8. R. Arnold et al. (SuperNEMO Collaboration), Probing new physics models of neutrinoless double-beta decay with SuperNEMO. Eur. Phys. J. C **70**, 927 (2010)
9. E. Armengaud et al. (CUPID Collaboration), The CUPID-Mo experiment for neutrinoless double-beta decay: performance and prospects. Eur. Phys. J. C **80**, 44 (2020)
10. A. Agrawal et al. (The AMoRE Collaboration), Projected background and sensitivity of amore-ii. Eur. Phys. J. C **85**(1), 9 (2025). https://doi.org/10.1140/epjc/s10052-024-13516-9
11. I.C. Bandac et al. (CROSS Collaboration), The $0\nu2\beta$-decay CROSS experiment: preliminary results and prospects. JHEP **01**, 018 (2020)
12. D.Q. Adams et al. (The CUORE Collaboration), Search for Majorana neutrinos exploiting millikelvin cryogenics with CUORE. Nature **604**(7904), 53–58 (2022). https://doi.org/10.1038/s41586-022-04497-4
13. S. Abe, et al., Search for Majorana Neutrinos with the Complete KamLAND-Zen Dataset (2024). arXiv:2406.11438 [hep-ex]
14. G. Adhikari et al. (nEXO Collaboration), nEXO: neutrinoless double beta decay search beyond 10^{28} year half-life sensitivity. J. Phys. G **49**, 015104 (2022)
15. C. Adams et al. (NEXT Collaboration), Sensitivity of a tonne-scale NEXT detector for neutrinoless double beta decay searches. JHEP **2021**(08), 164 (2021)
16. X. Chen et al. (PandaX Collaboration), PandaX-III: searching for neutrinoless double beta decay with high pressure ^{136}Xe gas time projection chambers. Sci. China Phys. Mech. Astron. **60**(6), 061011 (2017)
17. D.S. Akerib et al. (LZ Collaboration), Projected sensitivity of the LUX-ZEPLIN experiment to the $0\nu\beta\beta$ decay of ^{136}Xe. Phys. Rev. C **102**, 014602 (2020)
18. P. Pirinen, J. Suhonen, Systematic approach to β and $2\nu\beta\beta$ decays of mass $A = 100 - 136$ nuclei. Phys. Rev. C **91**, 054309 (2015). https://doi.org/10.1103/PhysRevC.91.054309
19. F.F. Deppisch, J. Suhonen, Statistical analysis of β decays and the effective value of g_A in the proton-neutron quasiparticle random-phase approximation framework. Phys. Rev. C **94**, 055501 (2016). https://doi.org/10.1103/PhysRevC.94.055501
20. J. Suhonen, *From Nucleons to Nucleus: Concepts of Microscopic Nuclear Theory* (Springer, Berlin, 2007)
21. S. Eliseev, T. Eronen, Y.N. Novikov, Penning-trap mass spectrometry for neutrino physics. Int. J. Mass Spectrom. **349–350**, 102–106 (2013). https://doi.org/10.1016/j.ijms.2013.03.010
22. S. Eliseev, Y. Novikov, High-precision Penning-trap mass spectrometry for neutrino physics. Eur. Phys. J. A **59** (2023). https://doi.org/10.1140/epja/s10050-023-00946-4
23. D.A. Nesterenko, L. Jokiniemi, J. Kotila, A. Kankainen, Z. Ge, T. Eronen, S. Rinta-Antila, J. Suhonen, High-precision Q-value measurement and nuclear matrix element calculations for the double-β decay of ^{98}Mo. Eur. Phys. J. A **58** (2022). https://doi.org/10.1140/epja/s10050-022-00695-w
24. K. Gulyuz, J. Ariche, G. Bollen, S. Bustabad, M. Eibach, C. Izzo, S.J. Novario, M. Redshaw, R. Ringle, R. Sandler, S. Schwarz, A.A. Valverde, Determination of the direct double-β-decay Q value of ^{96}Zr and atomic masses of $^{90-92,94,96}$Zr and $^{92,94--98,100}$Mo. Phys. Rev. C **91**, 055501 (2015). https://doi.org/10.1103/PhysRevC.91.055501
25. M. Eibach, G. Bollen, K. Gulyuz, C. Izzo, M. Redshaw, R. Ringle, R. Sandler, A.A. Valverde, Double resonant enhancement in the neutrinoless double-electron capture of ^{190}Pt. Phys. Rev. C **94**, 015502 (2016). https://doi.org/10.1103/PhysRevC.94.015502
26. S. Eliseev, K. Blaum, M. Block, C. Droese, M. Goncharov, E. Minaya Ramirez, D.A. Nesterenko, Y.N. Novikov, L. Schweikhard, Phase-imaging ion-cyclotron-resonance measurements for short-lived nuclides. Phys. Rev. Lett. **110**, 082501 (2013). https://doi.org/10.1103/PhysRevLett.110.082501
27. S. Eliseev, K. Blaum, M. Block, A. Dörr, C. Droese, T. Eronen, M. Goncharov, M. Höcker, J. Ketter, E.M. Ramirez, D.A. Nesterenko, Y.N. Novikov, L. Schweikhard, A phase-imaging technique for cyclotron-frequency measurements. Appl. Phys. B **114**(1), 107–128 (2014). https://doi.org/10.1007/s00340-013-5621-0
28. T. Eronen, V.S. Kolhinen, V.V. Elomaa, D. Gorelov, U. Hager, J. Hakala, A. Jokinen, A. Kankainen, P. Karvonen, S. Kopecky, I.D. Moore, H. Penttilä, S. Rahaman, S. Rinta-Antila, J. Rissanen, A. Saastamoinen, J. Szerypo, C. Weber, J. Äystö, JYFLTRAP: a Penning trap for precision mass spectroscopy and isobaric purification. Eur. Phys. J. A **48** (2012). https://doi.org/10.1140/epja/i2012-12046-1
29. I. Moore, T. Eronen, D. Gorelov, J. Hakala, A. Jokinen, A. Kankainen, V. Kolhinen, J. Koponen, H. Penttilä, I. Pohjalainen, M. Reponen, J. Rissanen, A. Saastamoinen, S. Rinta-Antila, V. Sonnenschein, J. Äystö, Towards commissioning the new IGISOL-4 facility. Nucl. Instrum. Methods Phys. Res. Sect. B **317**, 208–213 (2013). https://doi.org/10.1016/j.nimb.2013.06.036
30. J. Suhonen, On the double-beta decays of ^{70}Zn, ^{86}Kr, ^{94}Zr, ^{104}Ru, ^{110}Pd and ^{124}Sn. Nucl. Phys. A **864**(1), 63–90 (2011). https://doi.org/10.1016/j.nuclphysa.2011.06.021
31. M. Horoi, A. Neacsu, Shell model predictions for ^{124}Sn double-β decay. Phys. Rev. C **93**, 024308 (2016). https://doi.org/10.1103/PhysRevC.93.024308
32. J. Barea, J. Kotila, F. Iachello, Nuclear matrix elements for double-β decay. Phys. Rev. C **87**, 014315 (2013). https://doi.org/10.1103/PhysRevC.87.014315
33. J. Barea, J. Kotila, F. Iachello, $0\nu\beta\beta$ and $2\nu\beta\beta$ nuclear matrix elements in the interacting boson model with isospin restoration. Phys. Rev. C **91**, 034304 (2015). https://doi.org/10.1103/PhysRevC.91.034304

34. J. Menéndez, A. Poves, E. Caurier, F. Nowacki, Disassembling the nuclear matrix elements of neutrinoless $\beta\beta$ decay. Nucl. Phys. A **818**, 139–151 (2009). https://doi.org/10.1016/j.nuclphysa.2008.12.005
35. F. Šimkovic, V. Rodin, A. Faessler, P. Vogel, $0\nu\beta\beta$ and $2\nu\beta\beta$ nuclear matrix elements, quasiparticle random-phase approximation, and isospin symmetry restoration. Phys. Rev. C **87**, 045501 (2013). https://doi.org/10.1103/PhysRevC.87.045501
36. J. Hyvärinen, J. Suhonen, Nuclear matrix elements for $0\nu\beta\beta$ decays with light or heavy Majorana-neutrino exchange. Phys. Rev. C **91**, 024613 (2015). https://doi.org/10.1103/PhysRevC.91.024613
37. J. Hyvärinen, J. Suhonen, Analysis of the intermediate-state contributions to neutrinoless double β^- decays. Adv. High Energy Phys. **2016**, 4714829 (2016). https://doi.org/10.1155/2016/4714829
38. L. Jokiniemi, B. Soriano, J. Menéndez, Impact of the leading-order short-range nuclear matrix element on the neutrinoless double-beta decay of medium-mass and heavy nuclei. Phys. Lett. B **823**, 136720 (2021). https://doi.org/10.1016/j.physletb.2021.136720
39. J. Barea, J. Kotila, F. Iachello, Limits on neutrino masses from neutrinoless double-β decay. Phys. Rev. Lett. **109**, 042501 (2012). https://doi.org/10.1103/PhysRevLett.109.042501
40. F.F. Deppisch, L. Graf, F. Iachello, J. Kotila, Analysis of light neutrino exchange and short-range mechanisms in $0\nu\beta\beta$ decay. Phys. Rev. D **102**, 095016 (2020). https://doi.org/10.1103/PhysRevD.102.095016
41. E. Kauppinen, J. Kotila, Leading-order short-range nuclear matrix elements in double-β decay using the microscopic interacting boson model. Phys. Rev. C **112**, 034329 (2025). https://doi.org/10.1103/6y3v-5fww
42. T.R. Rodríguez, G. Martínez-Pinedo, Energy density functional study of nuclear matrix elements for neutrinoless $\beta\beta$ decay. Phys. Rev. Lett. **105**, 252503 (2010). https://doi.org/10.1103/PhysRevLett.105.252503
43. J.M. Yao, L.S. Song, K. Hagino, P. Ring, J. Meng, Systematic study of nuclear matrix elements in neutrinoless double-β decay with a beyond-mean-field covariant density functional theory. Phys. Rev. C **91**, 024316 (2015). https://doi.org/10.1103/PhysRevC.91.024316
44. J. Hyvärinen, J. Suhonen, Neutrinoless $\beta\beta$ decays to excited 0^+ states and the Majorana-neutrino mass. Phys. Rev. C **93**, 064306 (2016). https://doi.org/10.1103/PhysRevC.93.064306
45. J. Suhonen, M. Aunola, Systematic study of neutrinoless double beta decay to excited 0^+ states. Nucl. Phys. A **723**, 271–288 (2003). https://doi.org/10.1016/S0375-9474(03)01311-3
46. D.A. Nesterenko, T. Eronen, A. Kankainen, L. Canete, A. Jokinen, I.D. Moore, H. Penttilä, S. Rinta-Antila, A. de Roubin, M. Vilen, Phase-imaging ion-cyclotron-resonance technique at the JYFLTRAP double Penning trap mass spectrometer. Eur. Phys. J. A (2018). https://doi.org/10.1140/epja/i2018-12589-y
47. D.A. Nesterenko, T. Eronen, Z. Ge, A. Kankainen, M. Vilen, Study of radial motion phase advance during motion excitations in a penning trap and accuracy of JYFLTRAP mass spectrometer. Eur. Phys. J. A (2021). https://doi.org/10.1140/epja/s10050-021-00608-3
48. M. Vilén, L. Canete, B. Cheal, A. Giatzoglou, R. de Groote, A. de Roubin, T. Eronen, S. Geldhof, A. Jokinen, A. Kankainen, I. Moore, D. Nesterenko, H. Penttilä, I. Pohjalainen, M. Reponen, S. Rinta-Antila, A new off-line ion source facility at IGISOL. Nucl. Instrum. Methods Phys. Res. Sect. B **463**, 382–383 (2020). https://doi.org/10.1016/j.nimb.2019.04.051
49. A. Nieminen, J. Huikari, A. Jokinen, J. Äystö, P. Campbell, E. Cochrane, Beam cooler for low-energy radioactive ions. Nucl. Instrum. Methods Phys. Res. Sect. A **469**(2), 244–253 (2001). https://doi.org/10.1016/S0168-9002(00)00750-6
50. V. Virtanen, T. Eronen, A. Kankainen, O. Beliuskina, P. Campbell, R. Delaplanche, Z. Ge, R. de Groote, M. Hukkanen, A. Jaries, R. Kronholm, I. Moore, A. Raggio, A. de Roubin, J. Ruotsalainen, M. Schuh, Miniaturised cooler-buncher for reduction of longitudinal emittance at IGISOL. Nucl. Instrum. Methods Phys. Res. Sect. A **1072**, 170186 (2025). https://doi.org/10.1016/j.nima.2024.170186
51. G. Savard, S. Becker, G. Bollen, H.J. Kluge, R. Moore, T. Otto, L. Schweikhard, H. Stolzenberg, U. Wiess, A new cooling technique for heavy ions in a Penning trap. Phys. Lett. A **158**(5), 247–252 (1991). https://doi.org/10.1016/0375-9601(91)91008-2
52. A. Kramida, Yu. Ralchenko, J. Reader, NIST ASD Team, NIST Atomic Spectra Database (ver. 5.10) [Online]. `https://physics.nist.gov/asd` [2025, May 19]. National Institute of Standards and Technology, Gaithersburg (2022)
53. R.T. Birge, The calculation of errors by the method of least squares. Phys. Rev. **40**, 207–227 (1932). https://doi.org/10.1103/PhysRev.40.207
54. M. Wang, W. Huang, F. Kondev, G. Audi, S. Naimi, The AME 2020 atomic mass evaluation (II). Tables, graphs and references*. Chin. Phys. C **45**(3), 030003 (2021). https://doi.org/10.1088/1674-1137/abddaf
55. M.J. Bechara, O. Dietzsch, Q-values for (d, p) and (d, t) reactions on even-a tin isotopes. Zeitschrift für Naturforschung A **30**(3), 356–360 (1975). https://doi.org/10.1515/zna-1975-0315
56. M.R. Bhat, R.E. Chrien, G.W. Cole, O.A. Wasson, Neutron-capture gamma rays from ^{116}Sn and ^{122}Sn and the valence model. Phys. Rev. C **12**, 1457–1461 (1975). https://doi.org/10.1103/PhysRevC.12.1457
57. R.F. Carlton, S. Raman, G.G. Slaughter, Neutron capture gamma-ray studies of levels in ^{123}Sn and ^{125}Sn. Phys. Rev. C **15**, 883–893 (1977). https://doi.org/10.1103/PhysRevC.15.883
58. V. Bondarenko, T. von Egidy, J. Honzátko, I. Tomandl, D. Bucurescu, N. Marginean, J. Ott, W. Schauer, H.F. Wirth, C. Doll, Nuclear structure studies of 123te with (n,γ) and (d, p) reactions. Nucl. Phys. A **673**(1), 85–121 (2000). https://doi.org/10.1016/S0375-9474(00)00144-5
59. R. Firestone, S. Mughabghab, G. Molnar, *Database of Prompt Gamma Rays from Slow Neutron Capture for Elemental Analysis* (International Atomic Energy Agency, Vienna, 2006)
60. R. Georgii, T. von Egidy, J. Klora, H. Lindner, U. Mayerhofer, J. Ott, W. Schauer, P. von Neumann-Cosel, A. Richter, C. Schlegel, R. Schulz, V. Khitrov, A. Sukhovoj, A. Vojnov, J. Berzins, V. Bondarenko, P. Prokofjevs, L. Simonova, M. Grinberg, C. Stoyanov, Complete level scheme of ^{124}Te up to 3 MeV. Nucl. Phys. A **592**(3), 307–337 (1995). https://doi.org/10.1016/0375-9474(95)00311-N
61. T. von Egidy, H.F. Wirth, I. Tomandl, J. Honzátko, Complete (n, γ) level scheme of ^{124}Te. Phys. Rev. C **74**, 034319 (2006). https://doi.org/10.1103/PhysRevC.74.034319
62. D.A. Nesterenko, K. Blaum, M. Block, C. Droese, S. Eliseev, F. Herfurth, E. Minaya Ramirez, Y.N. Novikov, L. Schweikhard, V.M. Shabaev, M.V. Smirnov, I.I. Tupitsyn, K. Zuber, N.A. Zubova, Double-β transformations in isobaric triplets with mass numbers A=124, 130, and 136. Phys. Rev. C **86**, 044313 (2012). https://doi.org/10.1103/PhysRevC.86.044313
63. W. Huang, M. Wang, F. Kondev, G. Audi, S. Naimi, The AME 2020 atomic mass evaluation (i). Evaluation of input data, and adjustment procedures*. Chin. Phys. C **45**(3), 030002 (2021). https://doi.org/10.1088/1674-1137/abddb0
64. G. Gräff, H. Kalinowsky, J. Traut, A direct determination of the proton electron mass ratio. Zeitschrift für Physik A At. Nucl. **297**(1), 35–39 (1980). https://doi.org/10.1007/BF01414243
65. M. König, G. Bollen, H.J. Kluge, T. Otto, J. Szerypo, Quadrupole excitation of stored ion motion at the true cyclotron frequency. Int. J. Mass Spectrom. Ion Processes **142**(1), 95–116 (1995). https://doi.org/10.1016/0168-1176(95)04146-C
66. M. Kretzschmar, The Ramsey method in high-precision mass spectrometry with Penning traps: theoretical foundations. Int. J. Mass

Spectrom. **264**(2), 122–145 (2007). https://doi.org/10.1016/j.ijms.2007.04.002
67. S. George, K. Blaum, F. Herfurth, A. Herlert, M. Kretzschmar, S. Nagy, S. Schwarz, L. Schweikhard, C. Yazidjian, The Ramsey method in high-precision mass spectrometry with Penning traps: experimental results. Int. J. Mass Spectrom. **264**(2), 110–121 (2007). https://doi.org/10.1016/j.ijms.2007.04.003
68. S. Rahaman, V.V. Elomaa, T. Eronen, J. Hakala, A. Jokinen, A. Kankainen, J. Rissanen, J. Suhonen, C. Weber, J. Äystö, Double-beta decay Q values of ^{116}Cd and ^{130}Te. Phys. Lett. B **703**(4), 412–416 (2011). https://doi.org/10.1016/j.physletb.2011.07.078
69. N.D. Scielzo, S. Caldwell, G. Savard, J.A. Clark, C.M. Deibel, J. Fallis, S. Gulick, D. Lascar, A.F. Levand, G. Li, J. Mintz, E.B. Norman, K.S. Sharma, M. Sternberg, T. Sun, J. Van Schelt, Double-β-decay q values of ^{130}Te, ^{128}Te, and ^{120}Te. Phys. Rev. C **80**, 025501 (2009). https://doi.org/10.1103/PhysRevC.80.025501
70. M. Goncharov, K. Blaum, M. Block, C. Droese, S. Eliseev, F. Herfurth, E. Minaya Ramirez, Y.N. Novikov, L. Schweikhard, K. Zuber, Probing the nuclides ^{102}Pd, ^{106}Cd, and ^{144}Sm for resonant neutrinoless double-electron capture. Phys. Rev. C **84**, 028501 (2011). https://doi.org/10.1103/PhysRevC.84.028501
71. D. Nesterenko, L. Canete, T. Eronen, A. Jokinen, A. Kankainen, Y. Novikov, S. Rinta-Antila, A. de Roubin, M. Vilen, High-precision measurement of the mass difference between ^{102}Pd and ^{102}Ru. Int. J. Mass Spectrom. **435**, 204–208 (2019). https://doi.org/10.1016/j.ijms.2018.10.038
72. J. Ruotsalainen, E. Kauppinen, T. Eronen, A. Kankainen, J. Kotila, M. Mougeot, Probing the double-beta decay of ^{104}Ru through precise Q-value measurements and nuclear matrix element calculations. Eur. Phys. J. A **61**(2), 33 (2025). https://doi.org/10.1140/epja/s10050-024-01481-6
73. J. Kotila, F. Iachello, Phase-space factors for double-β decay. Phys. Rev. C **85**, 034316 (2012). https://doi.org/10.1103/PhysRevC.85.034316
74. F. Šimkovic, G. Pantis, J.D. Vergados, A. Faessler, Additional nucleon current contributions to neutrinoless double β decay. Phys. Rev. C **60**, 055502 (1999). https://doi.org/10.1103/PhysRevC.60.055502
75. F. Šimkovic, A. Faessler, H. Müther, V. Rodin, M. Stauf, $0\nu\beta\beta$-decay nuclear matrix elements with self-consistent short-range correlations. Phys. Rev. C **79**, 055501 (2009). https://doi.org/10.1103/PhysRevC.79.055501
76. R. Machleidt, F. Sammarruca, Y. Song, Nonlocal nature of the nuclear force and its impact on nuclear structure. Phys. Rev. C **53**, R1483 (1996). https://doi.org/10.1103/PhysRevC.53.R1483
77. B.A. Brown, N.J. Stone, J.R. Stone, I.S. Towner, M. Hjorth-Jensen, Magnetic moments of the 2_1^+ states around ^{132}Sn. Phys. Rev. C **71**, 044317 (2005). https://doi.org/10.1103/PhysRevC.71.044317
78. B.A. Brown, W. Rae, The shell-model code NuShellX@MSU. Nucl. Data Sheets **120**, 115 (2014). https://doi.org/10.1016/j.nds.2014.07.022
79. L. Jokiniemi, H. Ejiri, D. Frekers, J. Suhonen, Neutrinoless $\beta\beta$ nuclear matrix elements using isovector spin-dipole $J^\pi = 2^-$ data. Phys. Rev. C **98**, 024608 (2018). https://doi.org/10.1103/PhysRevC.98.024608
80. A. Bohr, B.R. Mottelson, *Nuclear Structure*, vol. I (Benjamin, New York, 1969)
81. K. Holinde, Two-nucleon forces and nuclear matter. Phys. Rep. **68**(3), 121–188 (1981). https://doi.org/10.1016/0370-1573(81)90188-5
82. P. Gimeno, L. Jokiniemi, J. Kotila, M. Ramalho, J. Suhonen, Ordinary muon capture on ^{136}Ba: comparative study using the shell model and pnQRPA. Universe **9**, 270 (2023). https://doi.org/10.3390/universe9060270
83. J. Menéndez, D. Gazit, A. Schwenk, Chiral two-body currents in nuclei: Gamow–Teller transitions and neutrinoless double-beta decay. Phys. Rev. Lett. **107**(6), 062501 (2011). https://doi.org/10.1103/physrevlett.107.062501
84. F. Iachello, A. Arima, *The Interacting Boson Model*. Cambridge Monographs on Mathematical Physics (Cambridge University Press, Cambridge, 1987). https://doi.org/10.1017/CBO9780511895517
85. J. Kotila, J. Barea, Occupation probabilities of single particle levels using the microscopic interacting boson model: application to some nuclei of interest in neutrinoless double-β decay. Phys. Rev. C **94**, 034320 (2016). https://doi.org/10.1103/PhysRevC.94.034320
86. V. Cirigliano, W. Dekens, J. de Vries, M.L. Graesser, E. Mereghetti, S. Pastore, U. van Kolck, New leading contribution to neutrinoless double-β decay. Phys. Rev. Lett. **120**, 202001 (2018). https://doi.org/10.1103/PhysRevLett.120.202001
87. R. Wirth, J.M. Yao, H. Hergert, Ab initio calculation of the contact operator contribution in the standard mechanism for neutrinoless double beta decay. Phys. Rev. Lett. **127**, 242502 (2021). https://doi.org/10.1103/PhysRevLett.127.242502
88. S. Abe et al. (KamLAND-Zen Collaboration), Search for the majorana nature of neutrinos in the inverted mass ordering region with KamLAND-Zen. Phys. Rev. Lett. **130**, 051801 (2023). https://doi.org/10.1103/PhysRevLett.130.051801
89. A. Belley, C.G. Payne, S.R. Stroberg, T. Miyagi, J.D. Holt, Ab initio neutrinoless double-beta decay matrix elements for ^{48}Ca, ^{76}Ge, and ^{82}Se. Phys. Rev. Lett. **126**, 042502 (2021)
90. L. Jokiniemi, B. Romeo, P. Soriano, J. Menéndez, Neutrinoless $\beta\beta$-decay nuclear matrix elements from two-neutrino $\beta\beta$-decay data. Phys. Rev. C **107**, 044305 (2023). https://doi.org/10.1103/PhysRevC.107.044305
91. V. Cirigliano, W. Dekens, J. de Vries, M.L. Graesser, E. Mereghetti, S. Pastore, M. Piarulli, U. van Kolck, R.B. Wiringa, Renormalized approach to neutrinoless double-β decay. Phys. Rev. C **100**, 055504 (2019). https://doi.org/10.1103/PhysRevC.100.055504